Mathematical Biosciences and Engineering

https://www.aimspress.com/journal/mbe

MBE, 23(7): 2083–2109.
DOI: 10.3934/mbe.2026076
Received: 22 April 2026
Revised: 29 May 2026
Accepted: 23 June 2026
Published: 13 July 2026

Research article

Learning contact policies for SEIR epidemics on networks: A mean-field game approach

Weinan Wang*

Department of Mathematics, University of Oklahoma, Norman, OK, USA

* **Correspondence:** Email: ww@ou.edu.

Abstract: In this paper, we develop a mean-field game model for SEIR epidemics on heterogeneous contact networks, where individuals choose state-dependent contact effort to balance infection losses against the social and economic costs of isolation. The Nash equilibrium is characterized by a coupled Hamilton–Jacobi–Bellman/Kolmogorov system across degree classes. An important feature of the SEIR setting is the exposed compartment: the incubation period separates infection from infectiousness and changes incentives after infection occurs. In the baseline formulation, exposed agents optimally maintain full contact, while susceptible agents reduce contact according to an explicit best-response rule driven by infection pressure and the value gap. We also discuss extensions that yield nontrivial exposed precaution by introducing responsibility or compliance incentives. We establish existence of equilibrium via a fixed-point argument and prove the uniqueness under a suitable monotonicity condition. The analysis identifies a delay in the onset of precaution under longer incubation, which can lead to weaker behavioral responses and larger outbreaks. Numerical experiments illustrate how network degree and the cost exponent shape equilibrium policies and epidemic outcomes.

Keywords: mean-field games; SEIR epidemic model; heterogeneous networks; Nash equilibrium; strategic delay; behavioral epidemiology

1. Introduction

Classical compartmental epidemic models, dating back to the seminal work of Kermack and McKendrick, treat contact rates as exogenous parameters and focus on the resulting population-level dynamics [1, 2]. In practice, contact behavior responds to perceived risk, information, and policies, producing feedback between disease prevalence and transmission opportunities [3–5]. This feedback can substantially alter epidemic trajectories and can also bias inference and forecasting when it is ignored [5, 6]. A complementary perspective models individual choices explicitly, for instance, through differential-game or game-theoretic formulations of distancing or protection [7, 8]. Network structure provides an additional layer of heterogeneity that is crucial for both transmission and behavior. A large literature shows how degree distributions, correlations, and mixing patterns reshape epidemic thresholds, early growth, and final size [9–14]. In particular, degree-structured and correlated networks are naturally encoded through $P(k)$ and $P(k'|k)$, which allow one to represent heterogeneous connectivity and assortativity in a tractable way [10, 13].

Mean-field game (MFG) theory offers a principled framework for modeling large populations of interacting decision makers, where each agent optimizes an individual objective against an aggregate state [15–18]. From a computational standpoint, forward–backward schemes and related finite-difference/iterative methods are standard tools for MFG systems [19]. Moreover, the interpretation of equilibrium computation as a learning procedure has become increasingly relevant for policy and behavioral applications [20, 21]. In epidemic modeling, several works have used MFG or mean-field equilibrium ideas to study contact reduction and the inefficiency gap between individual and socially optimal responses [22–26]. A complementary control-theoretic direction steers stochastic compartmental epidemic models by PDE-constrained control of the associated Fokker–Planck equation; cf [27]. Existing network-based MFG epidemic models have largely focused on SIR-type dynamics [26]. For pathogens with a meaningful latent period, with SARS-CoV-2 as a motivating example, the exposed compartment matters: infection and infectiousness are separated in time, and pre-symptomatic transmission can be significant [28]. This separation changes incentives after infection occurs, and it interacts with network heterogeneity in ways that are not present in SIR-based models.

In this paper, we develop a mean-field game framework for SEIR dynamics on heterogeneous networks. We derive the coupled HJB–Kolmogorov system across degree classes, using the compensator identity to represent a one-time infection loss as an equivalent running cost [29]. We show that in the baseline formulation exposed agents optimally maintain full contact, and we discuss extensions that yield nontrivial exposed precaution through responsibility or compliance incentives. We prove existence of equilibrium via a Schauder fixed-point argument and provide uniqueness under a suitable monotonicity condition. The analysis identifies an incubation-induced delay in the onset of precaution when the latent period is longer, which can lead to weaker equilibrium contact reductions and larger outbreaks. Numerical experiments illustrate how network degree and the isolation-cost exponent shape equilibrium policies and epidemic outcomes.

1.1. Related works

Behavioral responses in epidemics have been widely modeled through risk-dependent transmission and information-driven behavior, with surveys and systematic reviews summarizing many mechanisms and modeling choices [3, 4]. Game-theoretic treatments of protective behavior include vaccination and distancing models that expose free-riding and externalities [7, 8], as well as broader reviews of game-theoretic infectious-disease modeling [30] and data-driven optimal-control approaches to compartmental epidemic models [31]. On the network side, a broad theory connects epidemic dynamics to degree heterogeneity and mixing structure; see [9, 11, 14] and the degree-based random network formulation in [10, 12]. Correlations encoded by $P(k'|k)$ (Markovian networks) are known to alter thresholds and equilibrium conditions [13].

For MFG theory and computation, we refer to the foundational and modern references [15–19]. Learning-based viewpoints for equilibrium computation include fictitious play and mean-field reinforcement learning [20, 21]. In epidemic applications, mean-field equilibrium approaches to contact reduction and policy comparison are developed in [22, 23] and in social-structure models in [24–26]. More recent work has begun to extend mean-field and SEIR-type formulations to network and dynamic-network settings [32, 33], reflecting a rapidly expanding literature on behavior-coupled epidemic dynamics on networks. Related data-driven prediction and learning-based control methods for spreading and networked dynamical systems provide complementary tools for learning or approximating behavior-coupled models [34, 35]. The present paper differs by focusing on SEIR dynamics on heterogeneous networks and by isolating how the exposed compartment reshapes equilibrium incentives and timing.

2. The SEIR network model

We consider a population of N individuals (N large) situated on a network where nodes represent individuals and edges represent potential transmission contacts. Each individual has degree k (number of neighbors) drawn from distribution $P(k)$. Following the approach of Bremaud et al. [26], we consider Markovian networks characterized by $P(k)$ and the degree correlation matrix $G_{kk'} = P(k'|k)$. For the numerical experiments, we consider uncorrelated Markovian networks, for which $G_{kk'} = k'P(k')/\langle k\rangle$ and the force of infection reduces to $\Theta_k(t) \equiv \Theta(t)$, independent of degree class. Specifically, we take $P(k)$ to be a truncated Poisson distribution with mean $\mu = 8$ supported on $\{1, \dots, 25\}$, which gives $\langle k^2\rangle/\langle k\rangle = \mu + 1 = 9$ and allows $R_0 = \beta(\mu + 1)/\gamma$ to be set explicitly.

2.1. Compartmental dynamics

Individuals can be in one of four states: Susceptible (S), Exposed (E), Infectious (I), or Recovered (R). Let $S_k(t)$, $E_k(t)$, $I_k(t)$, and $R_k(t)$ denote the fractions of individuals with degree k in each state at time t, with normalization $S_k(t) + E_k(t) + I_k(t) + R_k(t) = 1$. The disease progression follows standard SEIR dynamics with network-dependent transmission:

$$\dot{S}_k(t) = -\lambda_k(t)S_k(t), \tag{2.1}$$

$$\dot{E}_k(t) = \lambda_k(t)S_k(t) - \sigma E_k(t), \tag{2.2}$$

$$\dot{I}_k(t) = \sigma E_k(t) - \gamma I_k(t),$$

$$\dot{R}_k(t) = \gamma I_k(t), \tag{2.3}$$

where σ^{-1} is the mean incubation period, and γ is the recovery rate.

2.2. Network-dependent force of infection

We incorporate network structure through the degree correlation matrix $G_{kk'} = P(k'|k)$ (Markovian networks). Let $\Theta_k(t)$ denote the probability that a randomly chosen neighbor of a degree-k node is effectively infectious. In the baseline SEIR setting, only infectious individuals transmit. Infectious individuals do not optimize their contact rate (they have no further incentive to reduce contacts and face no effort cost); we set $n_k^I \equiv 1$ for all k. The effective infection pressure from a randomly chosen neighbor of a degree-k node is therefore

$$\Theta_k(t) = \sum_{k'} G_{kk'}\, I_{k'}(t).$$

A susceptible individual of degree k has k neighbors, each contacted at effort $n_k^S(t)$, hence the force of infection is

$$\lambda_k(t) \;=\; \beta\, k\, n_k^S(t)\, \Theta_k(t). \tag{2.4}$$

Remark 2.1 (Why $n^I \equiv 1$)**.** *Once infectious, an individual has no remaining infection-risk incentive and faces no effort-cost term in* (3.4)*. Introducing n^I as a free variable without a corresponding cost would be internally inconsistent, so we set $n^I \equiv 1$. We emphasize that this is a modeling choice for the baseline, strategic, setting: it isolates the decisions of agents who still face infection risk (susceptible and exposed) from the dynamics of those already infected. In practice, infectious individuals often do reduce contact, either passively (illness, mandatory isolation) or actively (social responsibility). Such effects are not behavioral responses to infection risk but exogenous or externality-driven reductions; they can be incorporated by adding an effort-cost term in state I, or, in the case of pre-symptomatic transmission, through the responsibility/compliance extension discussed in Remark 3.5.*

If exposed individuals transmit at reduced rate $\beta_E = \kappa\beta$ with $\kappa \in [0, 1]$, then we instead set

$$\Theta_k(t) \;=\; \sum_{k'} G_{kk'}\Big(I_{k'}(t) + \kappa\, n_{k'}^E(t) E_{k'}(t)\Big), \tag{2.5}$$

and keep (2.4) unchanged.

If the network is uncorrelated, $G_{kk'} = \frac{k' P(k')}{\langle k \rangle}$, so $\Theta_k(t)$ becomes independent of k:

$$\Theta(t) \;=\; \frac{1}{\langle k \rangle} \sum_{k'} k' P(k')\, I_{k'}(t), \qquad \lambda_k(t) = \beta\, k\, n_k^S(t)\, \Theta(t). \tag{2.6}$$

2.3. Some assumptions

Assumption 2.2 (Control in the exposed compartment)**.** *We allow exposed individuals to choose a contact level $n_k^E(t) \in [\mathfrak{n}_{\min}, 1]$ to model awareness, compliance, or quarantine decisions. Under the baseline cost structure and purely symptomatic transmission, however, the exposed-state control does not affect the agent's own transition intensity, and the Nash best response is $n_k^{E*}(t) = 1$ (see* (3.8) *and Remark 3.5). Nontrivial exposed precautions ($n_k^{E*} < 1$) arise only under extensions that internalize pre-symptomatic transmission externalities or include responsibility/compliance penalties.*

Assumption 2.3 (Asymptomatic transmission)**.** *We consider two scenarios: (1) Exposed individuals are not infectious, with transmission occurring only from I individuals; (2) Exposed individuals can transmit at reduced rate $\beta_E = \kappa\beta$ with $0 \le \kappa \le 1$, reflecting pre-symptomatic transmission.*

3. Mean-field game formulation

3.1. Individual cost structure

Each individual of degree k aims to minimize an expected cost over time horizon $[0, T]$. The control variables are $(n^S(t), n^E(t))$, the contact-reduction efforts in states S and E respectively; in states I and R there is no active control ($n^I = n^R \equiv 1$). Throughout, "incentives" refers to the costs and benefits entering the individual objective (3.1): the social and economic cost of reduced contact (captured by f_k), the health costs C_E, C_I of being infected, and the lump-sum infection cost r_I. These may be interpreted as economic, social, or policy-driven, depending on the application. The individual cost is

$$J_k = \mathbb{E}\Bigg[\int_0^T \Big(r_I\,\lambda_k(t,n^S)\,\mathbb{I}_{\{x(t)=S\}} + f_k(n(t))\,\mathbb{I}_{\{x(t)\in\{S,E\}\}} \\ + C_E\,\mathbb{I}_{\{x(t)=E\}} + C_I\,\mathbb{I}_{\{x(t)=I\}}\Big)\,dt + \Psi(x(T))\Bigg], \tag{3.1}$$

where $n(t) = n^S(t)\,\mathbb{I}_{\{x(t)=S\}} + n^E(t)\,\mathbb{I}_{\{x(t)=E\}}$ is the state-dependent control, $f_k(\cdot)$ is the social/economic isolation cost, C_E, C_I are health costs, and Ψ is a terminal cost. Following Bremaud et al. [26], we take

$$f_k(n) = k^{\epsilon}\left(\frac{1}{n} - 1\right), \quad \epsilon \in \{0, 1\}.$$

Remark 3.1 (Infection lump-sum cost via the compensator identity)**.** *The term r_I represents a one-time cost paid at the (random) moment of infection $\tau = \inf\{t : x(t) = E\}$. By the Doob–Meyer compensator identity for a counting process with stochastic intensity $\lambda_k(t,n^S)\,\mathbb{I}_{\{x(t)=S\}}$,*

$$\mathbb{E}\big[r_I\,\mathbb{I}_{\{\tau\le T\}}\;\big|\;x(0)=S\big] = \mathbb{E}\left[\int_0^T r_I\,\lambda_k(t,n^S)\,\mathbb{I}_{\{x(t)=S\}}\,dt\;\middle|\;x(0)=S\right].$$

Writing it as a running cost inside the integral (rather than a terminal/stopping-time payment) is therefore exact and ensures the HJB equation (3.2) *is the correct necessary condition for the stated optimization problem. In particular, the jump term $r_I + U_k^E - U_k^S$ in* (3.2) *arises directly from differentiating this running cost.*

3.2. Value functions and HJB equations

Define the value function $U_k^x(t)$ as the minimum expected remaining cost for an individual of degree k in state x at time t:

$$U_k^x(t) = \min_{(n^S,n^E)} \mathbb{E}\Big[\int_t^T (r_I\lambda_k(s,n^S)\mathbb{I}_{\{x(s)=S\}} + f_k(n(s))\mathbb{I}_{\{x(s)\in\{S,E\}\}} \\ + C_E\mathbb{I}_{\{x(s)=E\}} + C_I\mathbb{I}_{\{x(s)=I\}})\,ds + \Psi(x(T))\;\Big|\;x(t)=x\Big].$$

Applying dynamic programming principles leads to the Hamilton-Jacobi-Bellman equations. For susceptible individuals,

$$-\frac{dU_k^S}{dt} = \min_{n^S\in[\mathfrak{n}_{\min},1]}\Big[\lambda_k(t,n^S)\left(r_I + U_k^E(t) - U_k^S(t)\right) + f_k(n^S)\Big], \tag{3.2}$$

where r_I is the infection cost incurred at the moment of infection, and $\lambda_k(t,n^S) = \beta k n^S\Theta_k(t)$. For exposed individuals,

$$-\frac{dU_k^E}{dt} = \min_{n^E\in[\mathfrak{n}_{\min},1]}\Big[\sigma\left(U_k^I(t) - U_k^E(t)\right) + C_E + f_k(n^E)\Big]. \tag{3.3}$$

Note that C_E enters (3.3) additively and does not depend on n^E; it therefore does not affect the optimal exposed effort n_k^{E*} (see Remark 3.5), and in the baseline case $C_E = 0$. For infectious and recovered individuals,

$$-\frac{dU_k^I}{dt} = \gamma\left(U_k^R(t) - U_k^I(t)\right) + C_I \tag{3.4}$$

$$-\frac{dU_k^R}{dt} = 0 \tag{3.5}$$

with terminal conditions $U_k^x(T) = \Psi(x)$. The terminal cost $\Psi(x)$ assigns a residual cost to each state at the end of the horizon; in the baseline model, we take $\Psi \equiv 0$, i.e., $\Psi(S) = \Psi(E) = \Psi(I) = \Psi(R) = 0$, so that all costs are accrued within $[0, T]$. Equation (3.5) reflects that a recovered agent incurs no further isolation or infection cost (no effort is exerted and no transitions remain); with $\Psi \equiv 0$ this gives $U_k^R \equiv 0$, so the recovered value is constant in time. A nonzero Ψ (e.g., a vaccination reward or a residual health cost) can be incorporated without changing the analysis.

3.3. Rigorous derivation of HJB equations

Theorem 3.2 (HJB Derivation for SEIR-MFG)**.** *The value functions $U_k^x(t)$ defined in (3.2) satisfy the HJB equations (3.2)–(3.5) under appropriate regularity conditions.*

Proof. We derive the HJB equation for susceptible individuals in detail; the other cases follow similarly. Consider a susceptible individual of degree k at time t. By the dynamic programming principle for a small time increment $h > 0$, and using the compensator identity for r_I (Remark 3.1):

$$\begin{aligned} U_k^S(t) = \min_{n^S(\cdot)} \mathbb{E}\Big[\int_t^{t+h} & \Big(r_I \lambda_k(s, n^S)\mathbb{I}_{\{x(s)=S\}} + f_k(n^S(s))\mathbb{I}_{\{x(s)\in\{S,E\}\}} \\ & + C_E \mathbb{I}_{\{x(s)=E\}} + C_I \mathbb{I}_{\{x(s)=I\}}\Big)\, ds \\ & + U_k^{x(t+h)}(t+h) \;\Big|\; x(t) = S\Big]. \end{aligned}$$

For sufficiently small h, the probability of multiple state transitions is $o(h)$. The individual remains susceptible with probability $1 - \lambda_k(t, n^S(t))h + o(h)$ and becomes exposed with probability $\lambda_k(t, n^S(t))h + o(h)$. Using the compensator representation of r_I, the dynamic programming principle gives

$$\begin{aligned} U_k^S(t) = \min_{n^S} \Big\{ & (r_I \lambda_k(t, n^S) + f_k(n^S))h + \left(1 - \lambda_k(t, n^S)h\right) U_k^S(t+h) \\ & + \lambda_k(t, n^S)h\, U_k^E(t+h) + o(h)\Big\}. \end{aligned}$$

Rearranging and taking $h \to 0$,

$$\frac{U_k^S(t+h) - U_k^S(t)}{h} = \min_{n^S}\left\{ r_I \lambda_k(t, n^S) + f_k(n^S) + \lambda_k(t, n^S)\left(U_k^E(t+h) - U_k^S(t+h)\right)\right\} + o(1).$$

Taking the limit $h \to 0$,

$$-\frac{dU_k^S}{dt} = \min_{n^S}\left\{ \lambda_k(t, n^S)(r_I + U_k^E(t) - U_k^S(t)) + f_k(n^S)\right\},$$

which is exactly Eq (3.2). For exposed individuals, the derivation is similar, but accounts for the Markovian transition $E \to I$ with intensity σ:

$$U_k^E(t) = \min_{n^E} \left\{ (C_E + f_k(n^E))h + (1 - \sigma h)U_k^E(t+h) + \sigma h U_k^I(t+h) + o(h) \right\},$$

leading to

$$-\frac{dU_k^E}{dt} = \min_{n^E} \left\{ C_E + f_k(n^E) + \sigma \left(U_k^I(t) - U_k^E(t) \right) \right\},$$

which is Eq (3.3). The derivations for infectious and recovered states are straightforward since no optimization is involved in those states (once infectious, the disease progression is autonomous).

3.4. Optimal effort policies

Definition 3.3 (Degree-scaled infection pressure)**.** *Define $\bar{\theta}_k(t) := k\,\Theta_k(t)$, so that the force of infection takes the compact form*

$$\lambda_k(t, n^S) = \beta\, n^S\, \bar{\theta}_k(t).$$

In the uncorrelated case, $\bar{\theta}_k(t) = k\,\Theta(t)$ with $\Theta(t)$ given by (2.6)*.*

The optimal effort levels are obtained from the minimization in the HJB equations. For susceptible individuals,

$$n_k^{S*}(t) = \arg \min_{n^S \in [\mathrm{n}_{\min}, 1]} \left[\beta n^S \bar{\theta}_k(t) \left(r_I + U_k^E(t) - U_k^S(t) \right) + f_k(n^S) \right].$$

Theorem 3.4 (Closed-form optimal control)**.** *For the social cost function $f_k(n) = k^{\epsilon}\left(\frac{1}{n} - 1\right)$, the optimal effort for susceptible individuals is*

$$n_k^{S*}(t) = \begin{cases} 1, & \bar{\theta}_k(t)\,\Delta U_k(t) \le 0, \\ \min\left\{ 1,\ \max\left\{ \mathrm{n}_{min},\ \sqrt{\dfrac{k^{\epsilon}}{\beta\,\bar{\theta}_k(t)\,\Delta U_k(t)}} \right\} \right\}, & \bar{\theta}_k(t)\,\Delta U_k(t) > 0, \end{cases} \tag{3.6}$$

where $\Delta U_k(t) := r_I + U_k^E(t) - U_k^S(t)$. Since $\bar{\theta}_k(t) = k\,\Theta_k(t)$, this is equivalently

$$n_k^{S*}(t) = \min\left\{ 1,\ \max\left\{ \mathrm{n}_{min},\ \sqrt{\frac{k^{\epsilon-1}}{\beta\,\Theta_k(t)\,\Delta U_k(t)}} \right\} \right\}. \tag{3.7}$$

(When $\Theta_k(t)\,\Delta U_k(t) \le 0$, the minimizer is $n_k^{S*}(t) = 1$ by monotonicity of the Hamiltonian in n.)

Proof. The minimization problem in (3.4) with $\lambda_k(t, n^S) = \beta n^S \bar{\theta}_k$ for interior solutions requires solving

$$\frac{\partial}{\partial n^S} \left[\beta n^S \bar{\theta}_k(t) \Delta U_k(t) + k^{\epsilon} \left(\frac{1}{n^S} - 1 \right) \right] = 0.$$

This gives

$$\beta \bar{\theta}_k(t) \Delta U_k(t) - \frac{k^{\epsilon}}{(n^S)^2} = 0.$$

Solving for n^S yields

$$n^S = \sqrt{\frac{k^\epsilon}{\beta\,\bar{\theta}_k(t)\,\Delta U_k(t)}}.$$

Substituting $\bar{\theta}_k = k\,\Theta_k$ recovers (3.7). The solution must be constrained to $[n_{\min}, 1]$, giving the result in (3.6).

For exposed individuals, under the current cost structure where transition to infectiousness is independent of contacts,

$$n_k^{E*}(t) = \arg\min_{n^E \in [n_{\min},1]} \left[f_k(n^E) \right] = 1 \quad \text{(since } f_k \text{ is decreasing in } n). \tag{3.8}$$

Remark 3.5 (Nash equilibrium value of n_k^{E*} and extensions)**.** *In the baseline model, the HJB equation* (3.3) *for an exposed individual minimizes only $f_k(n^E)$ (since the $\sigma(U_k^I - U_k^E)$ and C_E terms do not depend on n^E). Because f_k is decreasing, the Nash equilibrium strategy is $n_k^{E*} = 1$ for all t: an exposed agent who has no remaining infection risk and faces only an isolation penalty will not voluntarily self-isolate. When $\kappa > 0$ (pre-symptomatic transmission), exposed individuals' contact rate n_k^E enters the aggregate Θ_k through (2.5). However, at Nash equilibrium each individual optimizes against the* aggregate *field, not their own infinitesimal contribution. Therefore, $n_k^{E*} = 1$ continues to hold; the effect of $\kappa > 0$ is felt indirectly through the aggregate pressure on susceptibles.*

To obtain $n_k^{E*} < 1$ as a Nash outcome, one must add an incentive that increases *the exposed agent's running cost when n^E is large (high contacts). A simple choice is a responsibility/compliance term that internalizes pre-symptomatic transmission externalities, for example,*

$$\eta_E\,\kappa\beta\,k\,n^E(t)\,\Theta_k(t), \qquad \eta_E > 0,$$

added to the running cost in state E. Then, the exposed HJB becomes $\min_{n^E \in [n_{\min},1]} [\, \sigma(U_k^I - U_k^E) + C_E + f_k(n^E) + \eta_E \kappa\beta k n^E \Theta_k(t) \,]$, which admits interior minimizers and yields $n_k^{E*}(t) < 1$ when infection pressure is substantial.

3.5. Computing the reproduction number

In degree-structured network models, the effective reproduction number is most naturally defined via a next-generation operator acting on degree classes. In our setting (baseline: only I transmits), new exposures in class k generated by infectious individuals in class k' occur at instantaneous rate

$$\text{new } E_k \;\propto\; \beta\,k\,n_k^S(t)\,S_k(t)\,G_{kk'}\,n_{k'}^I(t)\,I_{k'}(t).$$

Theorem 3.6 (Time-varying effective reproduction number as a spectral radius)**.** *Define the $K \times K$ matrix*

$$\mathcal{K}(t)_{kk'} = \frac{\beta}{\gamma}\,k\,n_k^S(t)\,S_k(t)\,G_{kk'}.$$

Then the time-varying effective reproduction number is

$$R_t = \rho(\mathcal{K}(t)), \tag{3.9}$$

where $\rho(\cdot)$ denotes the spectral radius.

Remark 3.7 (R_t is the effective reproduction number)**.** *We emphasize that R_t in* (3.9) *is the* effective *(time-varying) reproduction number, which by definition incorporates the current susceptible fractions $S_k(t)$: it counts the expected secondary infections produced by a typical infectious individual* given the current state of the population*, including depletion of susceptibles and the prevailing equilibrium effort $n_k^S(t)$. This is the standard next-generation construction with the susceptible state evaluated at time t rather than at the disease-free equilibrium. The* basic *reproduction number R_0 is recovered as the special case $S_k \approx 1$, $n_k^S \equiv 1$ at the disease-free equilibrium, as stated in Corollary 3.8 below. The early-phase exponential growth rate is a distinct quantity and is treated separately in Proposition 5.6.*

Proof. We linearize the infection subsystem around the current state $(S_k(t))_{k=1}^K$ and consider a small perturbation in infectious mass $(I_{k'})_{k'=1}^K$. A degree-k' infectious individual remains infectious for mean time $1/\gamma$. During that time, it produces new exposures in class k along edges at rate $\beta\, k\, n_k^S(t)\, S_k(t)\, G_{kk'}$ (using $n^I \equiv 1$). Thus, the expected number of secondary cases in class k produced by one class-k' infectious is exactly $\mathcal{K}(t)_{kk'}$. The dominant growth/branching factor across degree classes is therefore the Perron root $\rho(\mathcal{K}(t))$, which yields (3.9).

Corollary 3.8 (Basic reproduction number at disease-free equilibrium)**.** *At the disease-free equilibrium $S_k(0) \approx 1$ and with baseline contact levels $n_k^S(0) = n_k^I(0) = 1$,*

$$R_0 \;=\; \rho(\mathcal{K}_0), \qquad (\mathcal{K}_0)_{kk'} = \frac{\beta}{\gamma}\, k\, G_{kk'}.$$

In the uncorrelated case $G_{kk'} = \frac{k' P(k')}{\langle k \rangle}$, $\mathcal{K}_0$ is rank-one and

$$R_0 \;=\; \frac{\beta}{\gamma}\,\frac{\langle k^2 \rangle}{\langle k \rangle}.$$

Remark 3.9 (Incubation rate σ and R_0)**.** *In the baseline SEIR model where only I transmits, the incubation rate σ affects timing (growth rate and peak), but not the expected number of secondary infections produced by one infected individual, hence R_0 depends on β, γ (and network structure) but not on σ.*

Remark 3.10. *For correlated networks, compute R_t by taking the largest eigenvalue of $\mathcal{K}(t)$ (power iteration is sufficient). For uncorrelated networks, the spectral radius reduces to the scalar*

$$R_t = \frac{\beta}{\gamma}\frac{1}{\langle k \rangle}\sum_k k^2 P(k)\, n_k^S(t)\, S_k(t).$$

4. Nash equilibrium characterization

4.1. Complete SEIR-MFG system

The MFG is characterized by the following coupled forward-backward system.

Forward (Kolmogorov) equations:

$$
\begin{aligned}
\dot{S}_k(t) &= -\beta k n_k^S(t)\Theta_k(t)S_k(t),\\
\dot{E}_k(t) &= \beta k n_k^S(t)\Theta_k(t)S_k(t) - \sigma E_k(t),\\
\dot{I}_k(t) &= \sigma E_k(t) - \gamma I_k(t),\\
\dot{R}_k(t) &= \gamma I_k(t),\\
\Theta_k(t) &= \sum_{k'} G_{kk'} I_{k'}(t).
\end{aligned}
$$

Backward (HJB) equations:

$$
\begin{aligned}
-\frac{dU_k^S}{dt} &= \beta k n_k^S(t)\Theta_k(t)\left(r_I + U_k^E(t) - U_k^S(t)\right) + f_k(n_k^S(t)),\\
-\frac{dU_k^E}{dt} &= \sigma\left(U_k^I(t) - U_k^E(t)\right) + C_E + f_k(n_k^E(t)),\\
-\frac{dU_k^I}{dt} &= \gamma\left(U_k^R(t) - U_k^I(t)\right) + C_I,\\
-\frac{dU_k^R}{dt} &= 0.
\end{aligned}
$$

Consistency conditions:

$$
n_k^S(t) = n_k^{S*}(t), \quad n_k^E(t) = n_k^{E*}(t),
$$

with initial conditions $S_k(0) \approx 1$, $E_k(0) = \varepsilon_k$, $I_k(0) = R_k(0) = 0$, and terminal conditions $U_k^x(T) = \Psi(x)$. The consistency condition (4.1) ensures that the effort parameters appearing in the population dynamics (FP) match those chosen by individuals optimizing against those same dynamics (HJB). This fixed-point condition defines the Nash equilibrium.

4.2. Existence and uniqueness

Theorem 4.1 (Existence of Nash equilibrium)**.** *Consider the SEIR-MFG system. Assume:*

1). *The social cost function $f_k(n)$ is strictly convex, twice continuously differentiable on $[\text{n}_{min}, 1]$, with $f_k'(n) < 0$ and $f_k''(n) > 0$.*

2). *Model parameters satisfy $0 < \beta, \sigma, \gamma < \infty$.*

3). *Initial conditions: $S_k(0) > 0$, $E_k(0), I_k(0), R_k(0) \geq 0$, with $S_k(0) + E_k(0) + I_k(0) + R_k(0) = 1$, and $\sum_k (E_k(0) + I_k(0)) > 0$ (nontrivial outbreak).*

4). *Degree distribution $P(k)$ has finite support $k \in \{1, 2, \ldots, K\}$.*

Then, there exists a Nash equilibrium on $[0, T]$.

We will prove the above theorem via a Schauder fixed point theorem. Note that the strategy of proving Nash equilibrium existence via a Schauder fixed-point argument on the policy space is standard in mean-field game theory [17] and has been applied in epidemic MFG settings by Hubert and Turinici [36] for SIR vaccination models and by Cecchin and Fischer [37] for MFG on graphs with congestion.

Proof. Since we have finitely many degree classes $k \in \{1, \dots, K\}$ and finite state space $\{S, E, I, R\}$, the state of the system is characterized by $4K$ continuous functions. We work in the Banach space

$$\mathcal{X} = C([0, T])^K \times C([0, T])^K$$

of pairs of continuous policies $(n^S(\cdot), n^E(\cdot))$ with $n_k^S, n_k^E : [0, T] \to [\mathfrak{n}_{\min}, 1]$, equipped with the sup-norm $\| \cdot \|_\infty$. Define

$$\mathcal{A} = \left\{ (n^S, n^E) \in \mathcal{X} : n_k^S(t),\ n_k^E(t) \in [\mathfrak{n}_{\min}, 1]\ \forall k, t \right\},$$

which is a closed, bounded, convex subset of $\mathcal{X}$. We continue in several steps.

Step 1 (Forward map is Lipschitz). Given $(n^S, n^E) \in \mathcal{A}$, the forward systems (2.1)–(2.3) is a system of ODEs with right-hand sides that are *uniformly Lipschitz* in the state (since $n_k^S \in [\mathfrak{n}_{\min}, 1]$ and all quantities are bounded). The Cauchy–Lipschitz theorem yields a unique solution $\mu[n] \in C^1([0, T])^{4K}$, bounded in $[\,0, 1\,]^{4K}$.

Step 2 (Backward map is Lipschitz). Given $\mu[n]$, the HJB systems (3.2)–(3.5) is a backward ODE with Lipschitz right-hand side (using the bounds on μ and n). The terminal-value problem has a unique solution $U[n] \in C^1([0, T])^{4K}$, uniformly bounded by $C_U := T(f_k(\mathfrak{n}_{\min}) + C_E + C_I) + \max |\Psi|$.

Step 3 (Best-response map). Define $\Phi : \mathcal{A} \to \mathcal{A}$ by

$$[\Phi(n)]_k^S(t) = \begin{cases} 1, & \bar{\theta}_k(t)\, \Delta U_k(t) \le 0, \\ \operatorname{proj}_{[\mathfrak{n}_{\min}, 1]}\left(\sqrt{\dfrac{k^\epsilon}{\beta\, \bar{\theta}_k(t)\, \Delta U_k(t)}} \right), & \bar{\theta}_k(t)\, \Delta U_k(t) > 0, \end{cases} \qquad [\Phi(n)]_k^E(t) \equiv 1.$$

where $\bar{\theta}_k, \Delta U_k$ are computed from Steps 1–2.

Step 4 (Compactness via Arzel'a–Ascoli). The image $\Phi(\mathcal{A})$ is equicontinuous. Indeed, $(\bar{\theta}_k(t))_k$ and $(\Delta U_k(t))_k$ are Lipschitz in t (solutions of Lipschitz ODEs). Define the clipped map

$$g(z) := \min\{1, \max\{\mathfrak{n}_{\min}, z^{-1/2}\}\}, \qquad z > 0,$$

and interpret it piecewise: $g(z) = 1$ for $z \le 1$, $g(z) = z^{-1/2}$ for $1 < z < 1/\mathfrak{n}_{\min}^2$, and $g(z) = \mathfrak{n}_{\min}$ for $z \ge 1/\mathfrak{n}_{\min}^2$. On each region g is Lipschitz, hence globally Lipschitz on $(0, \infty)$. Applying g to $z_k(t) := \beta\, \bar{\theta}_k(t)\, \Delta U_k(t)/k^\epsilon$ (with the convention $n^{S*} = 1$ if $z_k(t) \le 0$) yields a uniform modulus of continuity for $[\Phi(n)]_k^S(\cdot)$. Therefore, $\Phi(\mathcal{A})$ is relatively compact in $\mathcal{X}$ by Arzel'a–Ascoli.

Step 5 (Continuity of Φ). If $n^{(j)} \to n$ in $\mathcal{A}$ (uniform convergence), then by continuous dependence of the ODE solutions (Grönwall), $\mu[n^{(j)}] \to \mu[n]$ and $U[n^{(j)}] \to U[n]$ uniformly, so $\Phi(n^{(j)}) \to \Phi(n)$ uniformly.

$\mathcal{A}$ is a closed, bounded, convex subset of the infinite-dimensional space $\mathcal{X} = C([0, T])^{2K}$, but it is *not* compact (closed bounded convex sets in infinite-dimensional Banach spaces are not compact in general). What Steps 4–5 give instead is: $\Phi(\mathcal{A})$ is *relatively compact* (by Arzel–Ascoli) and Φ is continuous. By the Schauder fixed-point theorem in this form, a continuous map on a closed convex set whose image is relatively compact has a fixed point. Hence, Φ has a fixed point $n^* \in \mathcal{A}$, and $(\mu[n^*], n^*, U[n^*])$ is a Nash equilibrium.

Theorem 4.2 (Uniqueness under monotonicity conditions)**.** *Assume in addition to the conditions of Theorem 4.1 that*

1). *The Hamiltonian $H_k^S(n^S, U, \Theta_k)$ satisfies the displacement monotonicity condition: For any two sets of value functions $U^1, U^2 \in \mathcal{V}$ and corresponding infection pressures Θ^1, Θ^2,*

$$\sum_{k=1}^{K} \int_0^T \left[H_k^S(n_k^{S*1}, U_k^1, \Theta^1) - H_k^S(n_k^{S*2}, U_k^1, \Theta^1) - H_k^S(n_k^{S*1}, U_k^2, \Theta^2) + H_k^S(n_k^{S*2}, U_k^2, \Theta^2) \right] dt \geq 0,$$

with equality only when $n^{S*1} = n^{S*2}$ almost everywhere.

2). *The social cost $f_k(n)$ is strongly convex: $f_k''(n) \geq \alpha > 0$ for all $n \in [\mathrm{n}_{min}, 1]$.*

Then, the Nash equilibrium is unique.

Proof. Suppose there exist two distinct Nash equilibria (μ^1, n^1, U^1) and (μ^2, n^2, U^2). Denote differences by $\delta S_k = S_k^1 - S_k^2$, $\delta n_k^S = n_k^{S1} - n_k^{S2}$, $\delta U_k^S = U_k^{S1} - U_k^{S2}$, etc. From the optimality conditions,

$$\begin{aligned} n_k^{S1}(t) &= \arg\min_{n^S} H_k^S(n^S, U_k^1(t), \Theta^1(t)), \\ n_k^{S2}(t) &= \arg\min_{n^S} H_k^S(n^S, U_k^2(t), \Theta^2(t)). \end{aligned}$$

By optimality, we have for almost every t,

$$H_k^S(n_k^{S1}, U_k^1, \Theta^1) - H_k^S(n_k^{S2}, U_k^1, \Theta^1) \leq 0, \tag{4.1}$$
$$H_k^S(n_k^{S2}, U_k^2, \Theta^2) - H_k^S(n_k^{S1}, U_k^2, \Theta^2) \leq 0. \tag{4.2}$$

Adding (4.1) and (4.2),

$$\left[H_k^S(n_k^{S1}, U_k^1, \Theta^1) - H_k^S(n_k^{S2}, U_k^1, \Theta^1) \right] + \left[H_k^S(n_k^{S2}, U_k^2, \Theta^2) - H_k^S(n_k^{S1}, U_k^2, \Theta^2) \right] \leq 0. \tag{4.3}$$

By strong convexity of f_k,

$$\begin{aligned} &H_k^S(n_k^{S1}, U_k^1, \Theta^1) - H_k^S(n_k^{S2}, U_k^1, \Theta^1) \\ &\geq \beta k \Theta^1(r_I + U_k^{E1} - U_k^{S1})(n_k^{S1} - n_k^{S2}) + f_k'(n_k^{S2})(n_k^{S1} - n_k^{S2}) + \frac{\alpha}{2}(n_k^{S1} - n_k^{S2})^2. \end{aligned}$$

Since n_k^{S2} minimizes $H_k^S(\cdot, U_k^2, \Theta^2)$, we have $f_k'(n_k^{S2}) = -\beta k \Theta^2(r_I + U_k^{E2} - U_k^{S2})$. Thus,

$$\text{LHS of (4.3)} \geq \beta k \left[\Theta^1(r_I + U_k^{E1} - U_k^{S1}) - \Theta^2(r_I + U_k^{E2} - U_k^{S2}) \right] (n_k^{S1} - n_k^{S2}) + \alpha(n_k^{S1} - n_k^{S2})^2.$$

From the forward equations, we have

$$\frac{d}{dt}(\delta S_k) \leq C_1(|\delta n_k^S| + |\delta \Theta_k| + |\delta S_k|).$$

By Grönwall's inequality, $\|\delta S_k\|_{L^\infty} \leq C_2 \int_0^T (|\delta n_k^S| + |\delta \Theta_k|) dt$. For the value functions, from the HJB equations,

$$\left| \frac{d}{dt}(\delta U_k^S) \right| \leq C_3(|\delta n_k^S| + |\delta U_k^S| + |\delta U_k^E| + |\delta \Theta_k|).$$

Integrating backward gives $\|\delta U_k^S\|_{L^\infty} \leq C_4 \int_0^T(|\delta n_k^S|+|\delta\Theta_k|)dt$. The infection pressure difference satisfies that

$$|\delta\Theta_k(t)| \leq C_5 \sum_{k'} |\delta I_{k'}(t)|,$$

and from the I_k equation, $|\delta I_k(t)| \leq C_6 \int_0^t(|\delta E_k(s)| + |\delta I_k(s)|)ds$. Combining all estimates with the monotonicity condition yields

$$\alpha \sum_{k=1}^{K} \int_0^T |\delta n_k^S(t)|^2 dt \leq C_7 \sum_{k=1}^{K} \int_0^T |\delta n_k^S(t)| \cdot \left(\int_0^T |\delta n_k^S(s)| ds \right) dt.$$

Writing $a_k := \int_0^T |\delta n_k^S(t)|\, dt$ and applying the Cauchy–Schwarz inequality $a_k \leq T^{1/2}\big(\int_0^T |\delta n_k^S|^2\big)^{1/2}$ to the right-hand side gives $\alpha \sum_k \|\delta n_k^S\|_{L^2}^2 \leq C_7 T^{1/2} \sum_k \|\delta n_k^S\|_{L^2}\, a_k \leq C_7 T \sum_k \|\delta n_k^S\|_{L^2}^2$. When T is small enough that $C_7 T < \alpha$, this forces $\sum_k \|\delta n_k^S\|_{L^2}^2 = 0$; the restriction on T is then removed by iterating over successive subintervals of length $O(\alpha/C_7)$, a standard continuation argument. This is the network-SEIR adaptation of the monotonicity-based MFG uniqueness argument of Carmona and Delarue [17]. Applying Young's inequality and Grönwall's lemma gives $\delta n_k^S = 0$ almost everywhere. Then, $\delta\mu_k = 0$ and $\delta U_k = 0$ follow from the differential equations, establishing uniqueness.

Remark 4.3 (On the monotonicity condition)**.** *The displacement-monotonicity condition in Theorem 4.2 is a sufficient condition stated at the level of the Hamiltonian, in the spirit of standard MFG uniqueness theory [17]. We do not verify it analytically for the full SEIR-network Hamiltonian, since Θ_k depends nonlinearly on the state and ΔU_k may be non-monotone, particularly for small σ where the long incubation produces the late-time effort adjustments seen in Section 6. The uniqueness result should therefore be read as holding under appropriate monotonicity conditions; in all of our numerical experiments the forward–backward sweep converged to a single equilibrium regardless of initialization, consistent with uniqueness in the parameter regimes considered.*

4.3. Regularity of solutions

Lemma 4.4 (Boundedness and regularity)**.** *Under the assumptions of Theorem 1, the solutions satisfy,*

1). $S_k(t), E_k(t), I_k(t), R_k(t) \in [0,1]$ for all $t \in [0,T]$ and $\sum_{x\in\{S,E,I,R\}} X_k(t) = 1$.

2). $U_k^S(t), U_k^E(t), U_k^I(t), U_k^R(t)$ are uniformly bounded on $[0,T]$.

3). $n_k^{S*}(t), n_k^{E*}(t) \in [n_{min}, 1]$ and are measurable functions.

Proof. We see that the right-hand sides of (2.1)–(2.3) sum to zero:

$$\frac{d}{dt} \sum_{x\in\{S,E,I,R\}} X_k(t) = -\beta k n_k^S \Theta_k S_k + \beta k n_k^S \Theta_k S_k - \sigma E_k + \sigma E_k - \gamma I_k + \gamma I_k = 0,$$

so $\sum_x X_k(t) = \sum_x X_k(0) = 1$. Non-negativity follows from the structure of the equations. For the value functions,

$$|U_k^S(t)| \leq \int_t^T \left(\max_{n\in[\mathfrak{n}_{\min},1]} |f_k(n)| + C_E + C_I \right) ds + |\Psi(S)|$$
$$\leq T\left(\max_n |f_k(n)| + C_E + C_I\right) + \max_x |\Psi(x)|.$$

Similar bounds hold for U_k^E, U_k^I, U_k^R. The optimal controls are defined as minimizers of continuous functions over the compact set $[\mathfrak{n}_{\min}, 1]$, so they exist and are measurable by measurable selection theorems.

Theorem 4.5 (Continuous dependence on parameters)**.** *For two parameter sets $\mathcal{P}^1, \mathcal{P}^2$ with $\|\mathcal{P}^1 - \mathcal{P}^2\| \leq \delta$, the corresponding equilibria satisfy:*

$$\sup_{t\in[0,T]} \sum_{k=1}^K \left(|\mu_k^1(t) - \mu_k^2(t)| + |U_k^1(t) - U_k^2(t)| \right) + \int_0^T |n_k^1(t) - n_k^2(t)| dt \leq C(T, L)\delta,$$

where $C(T, L)$ depends on time horizon T and Lipschitz constants of the dynamics.

Proof. Let (μ^1, n^1, U^1) and (μ^2, n^2, U^2) be equilibria for parameters $\mathcal{P}^1$ and $\mathcal{P}^2$. Denote differences by $\delta\mu_k = \mu_k^1 - \mu_k^2$, $\delta n_k = n_k^1 - n_k^2$, $\delta U_k = U_k^1 - U_k^2$, $\delta\Theta_k = \Theta_k^1 - \Theta_k^2$. From the S_k equation, decomposing the difference,

$$\left|\frac{d}{dt}(\delta S_k)\right| \leq L_1(|\delta n_k^S| + |\delta\Theta_k| + |\delta S_k| + \delta),$$

since all quantities are bounded ($|n_k^S| \leq 1$, $|S_k| \leq 1$, $|\Theta_k| \leq 1$). For $\delta\Theta_k$,

$$|\delta\Theta_k(t)| \leq \frac{K \max k}{\langle k\rangle} \sum_{k'} |\delta I_{k'}|.$$

From the HJB for U_k^S,

$$\left|\frac{d}{dt}(\delta U_k^S)\right| \leq L_2(|\delta n_k^S| + |\delta\Theta_k| + |\delta U_k^S| + |\delta U_k^E| + \delta).$$

When solutions are interior, the first-order optimality conditions give $f_k'(n_k^{S\,i}) = -\beta k\Theta^i(r_I + U_k^{Ei} - U_k^{S\,i})$ for $i = 1, 2$. By the mean value theorem and strong convexity,

$$|\delta n_k^S| \leq \frac{L_3}{\alpha}(|\delta U_k^S| + |\delta U_k^E| + |\delta\Theta_k| + \delta).$$

Finally, we define

$$\Phi(t) = \sum_{k=1}^K \left(|\delta S_k(t)| + |\delta E_k(t)| + |\delta I_k(t)| + |\delta U_k^S(t)| + |\delta U_k^E(t)| \right).$$

Combining the estimates from Steps 1–3,

$$\frac{d\Phi}{dt} \le L_5(\Phi + \delta).$$

By Grönwall's inequality with $\Phi(0) \le C_0\delta$,

$$\Phi(t) \le C(T, L)\delta, \qquad \int_0^T |\delta n_k^S(t)| dt \le C'(T, L)\delta,$$

establishing the claimed continuous dependence.

5. Special cases and analytical insights

5.1. Strategic and biological roles of the incubation rate

The introduction of the exposed compartment reshapes the epidemic game through the value gap $\Delta U_k(t) = r_I + U_k^E(t) - U_k^S(t)$, the marginal cost of infection. As the following remark makes precise, σ acts on this gap through two opposing channels (Figure 1).

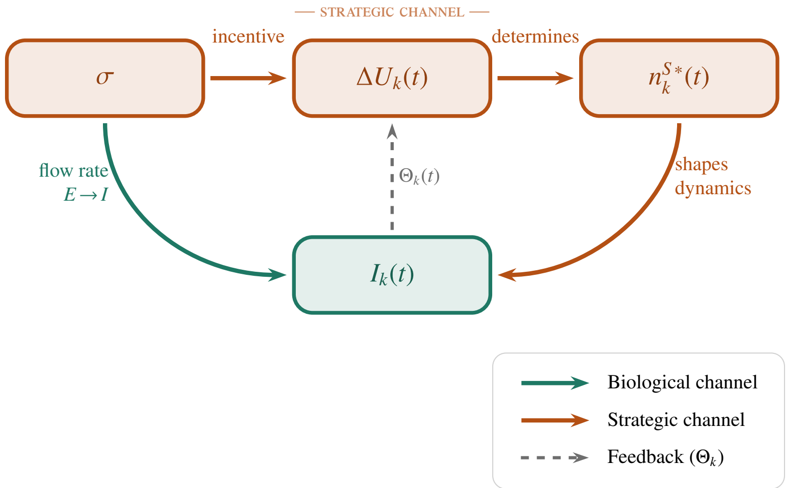

Figure 1. The dual role of incubation (σ). The incubation rate σ affects the epidemic through two distinct channels. **Biologically** (bottom arrow), it controls the flow rate from exposed to infectious ($\dot{I} \propto \sigma E$). **Strategically** (top arrow), it determines the immediacy of the infection cost, altering the value gap ΔU_k and thus the contact effort n_k^{S*}.

5.2. Degree scaling of optimal effort

For homogeneous networks where all nodes have degree k, the model yields clear analytical insights.

Proposition 5.1 (Degree scaling of optimal effort)**.** *Assume the uncorrelated reduction* (2.6) *and suppose the minimizer in the susceptible HJB is interior (i.e.,* $n_{\min} < n_k^{S*}(t) < 1$*). With*

$f_k(n) = k^\epsilon\left(\frac{1}{n} - 1\right)$, *we have*

$$n_k^{S*}(t) = \left(\frac{k^{\epsilon-1}}{\beta\,\Theta(t)\,\Delta U_k(t)}\right)^{1/2}, \qquad \Delta U_k(t) = r_I + U_k^E(t) - U_k^S(t). \tag{5.1}$$

Consequently:

- *if $\epsilon < 1$, then $n_k^{S*}(t)$ decreases with k (high-degree agents take* more *precaution);*
- *if $\epsilon = 1$, then $n_k^{S*}(t) = (\beta\,\Theta(t)\,\Delta U_k(t))^{-1/2}$ is* independent of *k;*
- *if $\epsilon > 1$, then $n_k^{S*}(t)$ increases with k (high-degree agents take* less *precaution).*

Degree thresholds appear only through saturation at the box constraints $[\mathfrak{n}_{\min}, 1]$.

Proof. With (2.4) and the uncorrelated reduction, the susceptible Hamiltonian is

$$H_k^S(n) = \beta\,k\,n\,\Theta(t)\,\Delta U_k(t) + k^\epsilon\Big(\frac{1}{n} - 1\Big).$$

For an interior minimizer, $0 = \partial_n H_k^S(n) = \beta k \Theta \Delta U_k - k^\epsilon/n^2$, hence $n^2 = k^{\epsilon-1}/(\beta\Theta\Delta U_k)$, which gives (5.1). The monotonicity conclusions follow immediately from the exponent $(\epsilon - 1)/2$.

Remark 5.2 (Minimized cost rate is linear in k for $\epsilon = 1$)**.** *Substituting the interior minimizer back for the case $\epsilon = 1$ gives*

$$H_k^*(t) = k\Big(2\sqrt{\beta\,\Theta(t)\,\Delta U_k(t)} - 1\Big).$$

This is linear *in k (assuming ΔU_k does not depend on k, which holds at zeroth order when degree effects on value functions are negligible). Therefore, no interior critical degree minimizes or maximizes the cost rate among interior-solution agents; differences across degree classes arise purely through the saturation behavior at the constraints $n^{S*} = \mathfrak{n}_{\min}$ or $n^{S*} = 1$.*

5.3. Comparison with SIR-MFG

The SEIR–SIR comparison has one rigorous early-growth component and one equilibrium-level observation supported by the numerical experiments. We state the rigorous early-growth comparison in Proposition 5.6 below (Section 5.4); here, we record the equilibrium-level numerical observation and its conditional consequence for the final outbreak size, keeping the proven and the numerically-observed statements clearly separated.

Remark 5.3 (Numerical attenuation of the SEIR response)**.** *In all numerical experiments in Section 6, the SEIR equilibrium response is delayed and shallower than the corresponding SIR response, in the sense that*

$$\max_t |1 - n^{\mathrm{SEIR}}(t)| \;\le\; \max_t |1 - n^{\mathrm{SIR}}(t)|.$$

This statement is reported as numerical evidence, not as a theorem. A proof would require comparing two different equilibrium forward–backward systems, as explained in Remark 5.5.

Proposition 5.4 (Conditional final-size comparison)**.** *Suppose that along the equilibrium trajectories the attenuated-response ordering $n^{\mathrm{SEIR}}(t) \ge n^{\mathrm{SIR}}(t)$ holds for all t (the pointwise form of the inequality in Remark 5.3), and that the two epidemics share the same initial susceptible mass. Then, the final-size relation* (5.2) *is consistent with, and in the numerical experiments yields, $R^{\mathrm{SEIR}}(\infty) \ge R^{\mathrm{SIR}}(\infty)$.*

Proof. Integrating $\dot{S}_k = -\beta k n^S \Theta_k S_k$ and using $\int_0^\infty I\,dt = R(\infty)/\gamma$ (which follows from $\dot{R} = \gamma I$) gives the final-size relation for both SEIR and SIR:

$$\ln \frac{S(0)}{S(\infty)} = \frac{\beta}{\gamma} \int_0^\infty n^S(t)\, I(t)\, dt. \tag{5.2}$$

Relation (5.2) holds separately for each model, with the model's own equilibrium effort n^S and infectious trajectory I appearing on the right-hand side. A weaker contact reduction (larger n^S) tends to increase the right-hand side and hence the cumulative outbreak $\ln(S(0)/S(\infty))$. A fully rigorous comparison is delicate because the infectious profile $I(t)$ also differs between the two models, so the right-hand side is coupled to $R(\infty)$ on both sides; we therefore state this as a conditional comparison rather than a strict inequality. In every numerical experiment of Section 6 the ordering $R^{\mathrm{SEIR}}(\infty) \geq R^{\mathrm{SIR}}(\infty)$ is observed, consistent with the weaker SEIR contact reduction documented there (see Table 1).

Remark 5.5 (Why the attenuated response is difficult to prove analytically)**.** *A natural attempt is to compare* $\Delta U^{SEIR} = r_I + U^E_{SEIR} - U^S_{SEIR}$ *with* $\Delta U^{SIR} = r_I + U^I_{SIR} - U^S_{SIR}$.

However, the naïve inequality $U^I_{SIR} \geq U^E_{SEIR}$ *is* not *obviously true, nor is its reverse. In fact, within the SEIR model itself, since being in state E means the agent must still pass through the E-sojourn (incurring cost* C_E*) before reaching I, the ordering* $U^E_{SEIR} \geq U^I_{SEIR}$ *holds. But, this is a within-model comparison, whereas the attenuated-response inequality of Remark 5.3 requires comparing value functions across two* different *games (SEIR-MFG vs SIR-MFG) with different population dynamics. A rigorous proof would require tracking how the equilibrium trajectories* $I^{SEIR}(t)$ *and* $I^{SIR}(t)$ *differ and propagating those differences back through the HJB. This is left for future work; numerical evidence in Section 6 consistently supports the claim.*

Note also that there is no discount factor in the HJB (3.2)–(3.5)*; the strategic delay effect arises from the finite horizon and the temporal structure of costs, not from exponential discounting.*

5.4. Early-phase growth rate comparison

Proposition 5.6 (Early-phase growth rate: SEIR is slower than SIR for the same contact level)**.** *Fix a constant contact level* $n^S \equiv \bar{n} \in (0, 1]$ *and consider the homogeneous mean-field dynamics with* $S(t) \approx 1$*. For SIR, the linearized growth rate is* $\lambda_{\mathrm{SIR}} = \beta\bar{n} - \gamma$*. For SEIR (baseline: only I transmits), the linearized growth rate is the largest root of*

$$\lambda^2 + (\sigma + \gamma)\lambda + \sigma(\gamma - \beta\bar{n}) = 0,$$

i.e.,

$$\lambda_{\mathrm{SEIR}} = \frac{-(\sigma + \gamma) + \sqrt{(\sigma + \gamma)^2 + 4\sigma(\beta\bar{n} - \gamma)}}{2}.$$

Whenever $\beta\bar{n} > \gamma$ *(supercritical regime), one has*

$$0 < \lambda_{\mathrm{SEIR}} < \lambda_{\mathrm{SIR}}.$$

Proof. The SIR formula is immediate from $\dot{I} = (\beta\bar{n} - \gamma)I$. For SEIR, linearizing gives $\dot{E} = \beta\bar{n}I - \sigma E$ and $\dot{I} = \sigma E - \gamma I$, so $\frac{d}{dt}\binom{E}{I} = A\binom{E}{I}$ with $A = \begin{pmatrix} -\sigma & \beta\bar{n} \\ \sigma & -\gamma \end{pmatrix}$. The characteristic polynomial is exactly $\lambda^2 + (\sigma + \gamma)\lambda + \sigma(\gamma - \beta\bar{n})$. In the supercritical regime $\beta\bar{n} > \gamma$, the Perron root is positive. A direct comparison of the explicit formulas yields $\lambda_{\mathrm{SEIR}} < \beta\bar{n} - \gamma$ for all finite σ.

5.5. Consequences of incubation for strategic incentives

Proposition 5.7 (Strategic delay in precaution onset). *In the supercritical regime, the optimal susceptible effort satisfies $n_k^{S*}(t) = 1$ on an initial interval $[0, t_\sigma^*)$. As σ decreases (longer incubation), t_σ^* increases.*

Proof. By (5.1), the interior solution $n_k^{S*} < 1$ requires $\beta\,\Theta(t)\,\Delta U_k(t) > k^{\epsilon-1}$. At $t = 0$ with $I(0) = \varepsilon \ll 1$, we have $\Theta(0) = O(\varepsilon)$, so $\beta\,\Theta(0)\,\Delta U_k(0) < k^{\epsilon-1}$ for small ε. Hence, $n_k^{S*}(0) = 1$. The threshold t_σ^* is defined by $\beta\,\Theta(t_\sigma^*)\,\Delta U_k(t_\sigma^*) = k^{\epsilon-1}$. Under the baseline definition $\Delta U_k(t) = r_I + U_k^E(t) - U_k^S(t)$, the gap is driven by the epidemic trajectory through the coupled backward HJB system. For smaller σ, $I_k(t)$ builds up more slowly (the mean E-sojourn time σ^{-1} must elapse before I grows), keeping $\Theta(t)$ smaller at early times. The product $\beta\,\Theta\,\Delta U_k$ therefore remains below $k^{\epsilon-1}$ for longer, so t_σ^* increases as σ decreases.

5.6. The SIR limit ($\sigma \to \infty$)

Lemma 5.8 (Convergence to SIR-MFG and the initial layer). *Fix all parameters except σ and suppose $C_E = 0$, $\Psi \equiv 0$. As $\sigma \to \infty$:*

(1) *If the initial exposed mass is compatible with the SIR limit, e.g., $E_k^\sigma(0) = O(\sigma^{-1})$, then $E_k^\sigma \to 0$ uniformly on $[0, T]$. If instead $E_k^\sigma(0) = E_k^0$ is fixed independently of σ, there is an initial layer of width $O(\sigma^{-1})$ near $t = 0$: for every $\delta > 0$, $\sup_{t\in[\delta,T]} E_k^\sigma(t) \to 0$, and the limiting SIR system should be initialized with $I_k^{\mathrm{SIR}}(0) = I_k^0 + E_k^0$ (up to the initial-layer correction).*

(2) $\|U_k^{E,\sigma} - U_k^{I,\sigma}\|_\infty \to 0$.

(3) $\Delta U_k^\sigma(t) \to \Delta U_k^{\mathrm{SIR}}(t) = r_I + U_k^{I,\infty}(t) - U_k^{S,\infty}(t)$ *uniformly on $[\delta, T]$ for every $\delta > 0$ (on all of $[0, T]$ under the compatibility condition in (1)).*

(4) *The SEIR-MFG Nash equilibrium converges to the SIR-MFG equilibrium of [26] at rate $O(\sigma^{-1})$ away from the initial layer.*

We note that, in either formulation, the limiting SIR-MFG model has the same *basic reproduction number $R_0 = \beta\langle k^2\rangle/(\gamma\langle k\rangle)$ as the SEIR model for every σ, since by Remark 3.9 the incubation rate σ affects only the timing of the epidemic and not R_0. The convergence above is therefore a convergence at fixed R_0, isolating the effect of the latent period.*

Proof. From (2.2), $\dot E_k = \lambda_k S_k - \sigma E_k$. By variation of constants,

$$E_k^\sigma(t) = e^{-\sigma t} E_k^\sigma(0) + \int_0^t e^{-\sigma(t-s)} \lambda_k^\sigma(s) S_k^\sigma(s)\, ds.$$

Since $\lambda_k^\sigma S_k^\sigma$ is uniformly bounded by some constant C, the integral term is bounded by C/σ. For $t \ge \delta > 0$,

$$E_k^\sigma(t) \;\le\; e^{-\sigma\delta} E_k^\sigma(0) + \frac{C}{\sigma} \;\longrightarrow\; 0,$$

which gives uniform convergence on $[\delta, T]$. The first term $e^{-\sigma t} E_k^\sigma(0)$ does not vanish uniformly on all of $[0, T]$ when $E_k^\sigma(0)$ is fixed (at $t = 0$ it equals $E_k^\sigma(0)$), producing the initial layer; uniform convergence on the whole interval holds precisely under the compatibility condition $E_k^\sigma(0) = O(\sigma^{-1})$. This establishes (1). Set $w_k = U_k^I - U_k^E$. Then, $w_k(T) = 0$ and

$$\dot{w}_k = \sigma w_k + [\gamma(U_k^R - U_k^I) + C_I].$$

The source is bounded uniformly in σ by the boundedness lemma. Integrating backward from T,

$$|w_k(t)| \leq \frac{M}{\sigma}(1 - e^{-\sigma(T-t)}) \leq \frac{M}{\sigma},$$

establishing (2). Then, $\Delta U_k^\sigma = r_I + U_k^{E,\sigma} - U_k^{S,\sigma} = r_I + U_k^{I,\sigma} - U_k^{S,\sigma} + O(\sigma^{-1})$. The limiting gap $r_I + U_k^{I,\infty} - U_k^{S,\infty}$ is the SIR-MFG value gap $\Delta U_k^{\mathrm{SIR}}$, establishing (3). Since $\Delta U_k^\sigma \to \Delta U_k^{\mathrm{SIR}}$ uniformly away from the initial layer, the optimal policy (5.1) converges $n_k^{S,\sigma} \to n_k^{S,\mathrm{SIR}}$; combined with (1), the forward dynamics converge to the SIR system, establishing (4).

6. Numerical simulations

We solve the coupled forward-backward SEIR-MFG system by a standard forward-backward sweep (FBS) iteration, alternating between (i) simulating the population dynamics forward in time under a candidate policy, (ii) solving the HJB system backward in time under the resulting epidemic trajectory, and (iii) updating the policy by pointwise minimization of the Hamiltonians. A relaxation parameter $\omega \in (0, 1]$ prevents oscillations.

6.1. Iterative forward-backward sweep algorithm

Fix a time grid $0 = t_0 < t_1 < \cdots < t_M = T$, a tolerance tol > 0, and a relaxation parameter $\omega \in (0, 1]$. Starting from $n_k^{S,(0)}(t_i) \equiv 1$, repeat the following steps until convergence.

Forward step. Given $n^{S,(m)}$, integrate the forward Kolmogorov system by explicit Euler with step Δt to obtain $(S_k^{(m+1)}, E_k^{(m+1)}, I_k^{(m+1)}, R_k^{(m+1)})$ and compute $\Theta_k^{(m+1)}(t)$. Because the SEIR right-hand side satisfies $\dot{S}_k + \dot{E}_k + \dot{I}_k + \dot{R}_k = 0$ identically, the explicit Euler scheme inherits mass conservation $S_k + E_k + I_k + R_k = 1$ to floating-point precision at every step, with no clipping or renormalization required.

Backward step. Solve the HJB system backward from t_M to t_0 by explicit Euler to obtain $(U_k^{S,(m+1)}, U_k^{E,(m+1)}, U_k^{I,(m+1)}, U_k^{R,(m+1)})$. Under the baseline parameters $C_E = C_I = 0$ and $\Psi \equiv 0$, one has $U_k^R \equiv U_k^I \equiv U_k^E \equiv 0$, so the value gap reduces to $\Delta U_k(t) = r_I - U_k^S(t)$ and only the backward equation for U_k^S is nontrivial.

Policy update. Compute the closed-form minimizer $\tilde{n}_k^{S,(m+1)}$ via (3.6), and apply relaxation:

$$n_k^{S,(m+1)} \leftarrow (1 - \omega)\, n_k^{S,(m)} + \omega\, \tilde{n}_k^{S,(m+1)}.$$

Stop when $\max_{k,i} |n_k^{S,(m+1)}(t_i) - n_k^{S,(m)}(t_i)| <$ tol.

6.2. Simulation setup

Heterogeneous-network experiment (primary). We simulate the full degree-structured model with an uncorrelated truncated Poisson degree distribution, $P(k) = e^{-\mu}\mu^k/k! / \sum_{j=1}^{K_{\max}} e^{-\mu}\mu^j/j!$, with mean degree $\mu = 8$ and truncation $K_{\max} = 25$. The transmission rate is set to $\beta = 0.44$ so that

$$R_0 = \frac{\beta}{\gamma}\frac{\langle k^2 \rangle}{\langle k \rangle} = \frac{\beta}{\gamma}(\mu + 1) = 4,$$

using the Poisson identity $\langle k^2\rangle/\langle k\rangle = \mu + 1$. All 25 degree classes are coupled through the shared infection pressure $\Theta(t) = \langle k\rangle^{-1} \sum_{k'} k' P(k') I_{k'}(t)$. The remaining parameters are $\gamma = 1$, $r_I = 50$, $\mathrm{n}_{\min} = 0.1$, $\varepsilon = 1$, $\Delta t = 0.05$, $\omega = 0.3$, and tol$= 10^{-7}$.

Homogeneous-network illustrations (secondary). Following [26], we also report results for homogeneous networks with $\beta k = 4$ fixed across degree classes $k \in \{4, 6, 8, 12, 20\}$. These runs should be interpreted as illustrations of the cost-normalization effect rather than as validation of the full degree-structured model: fixing βk removes the pure network-transmission heterogeneity, so degree differences manifest only through the isolation cost $f_k(n) = k^{\varepsilon}(1/n - 1)$. In particular, with $\varepsilon = 1$, larger k implies a larger cost factor $f_k = k$, which pushes the equilibrium effort $n_k^{S*} = \sqrt{k/(\beta_k I\, \Delta U)}$ upward toward 1 (weaker precaution), not downward.

6.3. Simulation results

Heterogeneous network. Figure 2 compares the aggregate and per-class SEIR-MFG and SIR-MFG Nash equilibria on the Poisson network at $\sigma = 2$. The aggregate SEIR epidemic (solid red) peaks later ($t^* \approx 3.75$) and lower than the SIR epidemic (dashed blue, $t^* \approx 1.75$). Per-class quantities reveal the network structure: high-degree nodes ($k = 18$) are infected more than low-degree nodes ($k = 2$) and, because $f_k = k$ is larger, exercise weaker equilibrium precaution.

Figure 3 shows the sensitivity of the heterogeneous-network equilibrium to the incubation rate σ. As σ decreases from 20 to 0.5, the epidemic peak shifts from $t^* \approx 2.0$ to $t^* \approx 7.2$ and the population-average effort $\bar{n}^{S*}(t) = \sum_k P(k) n_k^{S*}(t)$ becomes progressively shallower and delayed, directly illustrating the strategic delay mechanism of Proposition 5.7. The SIR limit ($\sigma \to \infty$, dashed black) produces the strongest and earliest behavioral response. The non-monotone "bump" in the population-average effort $\bar{n}^{S*}(t)$ at late times for $\sigma = 0.5$ and $\sigma = 1$ (Figure 3, right) is a feature of the coupled forward–backward structure: with a long incubation period, the infectious pressure $\Theta(t)$ persists late into the horizon, while the backward value functions adjust to the approaching terminal time T. As the value gap $\Delta U_k(t)$ relaxes near $t = T$, the best-response effort (3.6) partially returns toward 1, producing the secondary adjustment. It is a finite-horizon effect and not a steady-state property of the equilibrium. Table 1 summarizes peak timing and final outbreak size across σ values; all runs converge in 40–42 FBS iterations.

Table 1. Heterogeneous-network SEIR-MFG Nash equilibrium summary. Truncated Poisson $P(k)$, $\langle k\rangle = 8$, $R_0 = 4$, $\Delta t = 0.05$, $\omega = 0.3$, and tol $= 10^{-7}$.

σ	t_{peak}	$\max_t I_{\text{agg}}(t)$	$R(\infty) = 1 - S_{\text{agg}}(\infty)$
0.5	7.200	0.1201	0.9379
1.0	5.100	0.1789	0.9285
2.0	3.750	0.2384	0.9167
5.0	2.700	0.2989	0.9066
20.0	2.000	0.3405	0.9008
SIR ($\sigma \to \infty$)	1.750	0.3554	0.8987

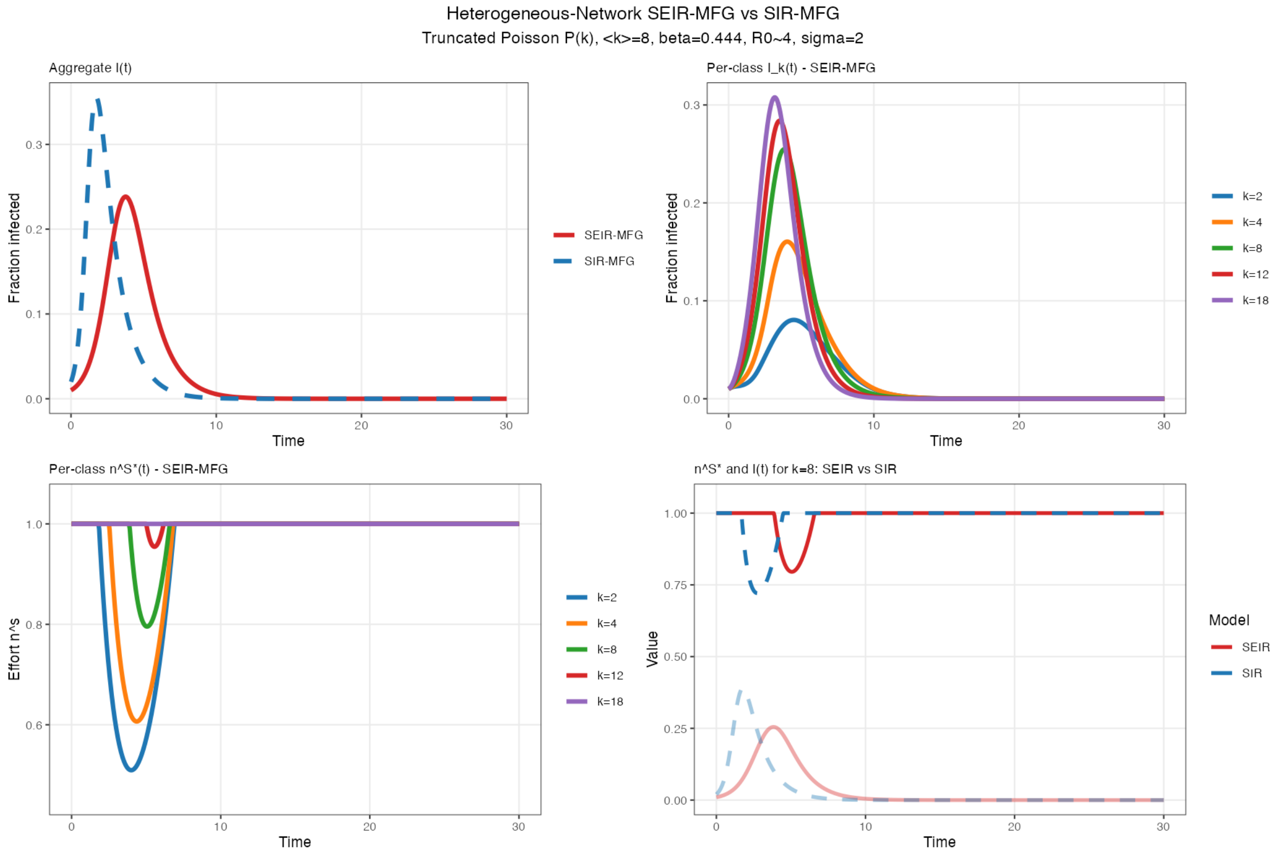

Figure 2. Nash equilibrium dynamics on the heterogeneous Poisson network ($\langle k\rangle = 8$, $R_0 = 4$, $\sigma = 2$). **Top-left:** aggregate infected fraction $I_{\text{agg}}(t)$ for SEIR-MFG (solid red) and SIR-MFG (dashed blue). **Top-right:** per-class $I_k(t)$ for selected degree classes under SEIR-MFG; higher-degree nodes are infected more due to the $\lambda_k \propto k$ scaling. **Bottom-left:** per-class equilibrium effort $n_k^{S*}(t)$; lower-degree nodes exercise stronger precaution because the isolation cost $f_k = k$ is smaller. **Bottom-right:** effort and infected fraction for $k = 8$, SEIR-MFG vs. SIR-MFG; the SEIR effort response is delayed and shallower, illustrating the strategic delay mechanism.

Homogeneous-network illustrations. Figure 4 presents the homogeneous-network results. The left panel shows that epidemic curves are nearly identical across degree classes, reflecting the fixed-βk normalization. The middle panel shows the effort profiles: larger k produces *weaker* precaution because the isolation cost $f_k = k$ dominates in the best-response formula; for $k = 20$, the equilibrium effort is $n_{20}^{S*} \equiv 1$ (no precaution, converged in 1 FBS iteration). The right panel illustrates the SEIR/SIR timing comparison for $k = 6$ and annotates the seed convention $I_0^{\text{SIR}} = I_0 + E_0$ used to ensure comparable initially infected mass; part of the SIR epidemic's earlier peak is therefore attributable to initialization. Table 2 records peak times, final sizes, and minimum effort levels for each degree class; all runs with $k \leq 12$ converge in 36–43 FBS iterations.

Figure 5 summarizes peak timing and final outbreak size across σ values. Two features of Table 1 are worth noting. First, both peak time and peak height decrease monotonically as σ increases toward the SIR limit, confirming that the exposed compartment delays and attenuates the epidemic through both the biological and strategic channels. Second, the final outbreak size $R(\infty)$ is *larger* for smaller σ even though the instantaneous peak is lower: weaker and later precaution allows more cumulative infections despite suppressing the peak.

Table 2. Homogeneous-network illustration summary ($\beta k = 4$, $\sigma = 2$, $\varepsilon = 1$). Note: larger k implies larger isolation cost $f_k = k$, and hence *weaker* equilibrium precaution.

k	$t^{\mathrm{SEIR}}_{\mathrm{peak}}$	$R^{\mathrm{SEIR}}(\infty)$	$\min_t n^{S*}_k(t)$	$t^{\mathrm{SIR}}_{\mathrm{peak}}$	$R^{\mathrm{SIR}}(\infty)$
4	3.600	0.9470	0.537	1.600	0.9258
6	3.750	0.9671	0.653	1.700	0.9564
8	3.750	0.9752	0.757	1.750	0.9695
12	3.750	0.9813	0.932	1.750	0.9795
20	3.750	0.9821	1.000†	1.750	0.9828

†For $k = 20$ with $\varepsilon = 1$, the isolation cost $f_{20} = 20$ dominates the infection-pressure term in the best-response formula for all t, yielding $n^{S*}_{20} \equiv 1$ (no precaution). Convergence is achieved in a single FBS iteration. The slight reversal $R^{\mathrm{SIR}}(\infty) > R^{\mathrm{SEIR}}(\infty)$ at $k = 20$ reflects this cost-normalization artifact rather than a genuine model prediction.

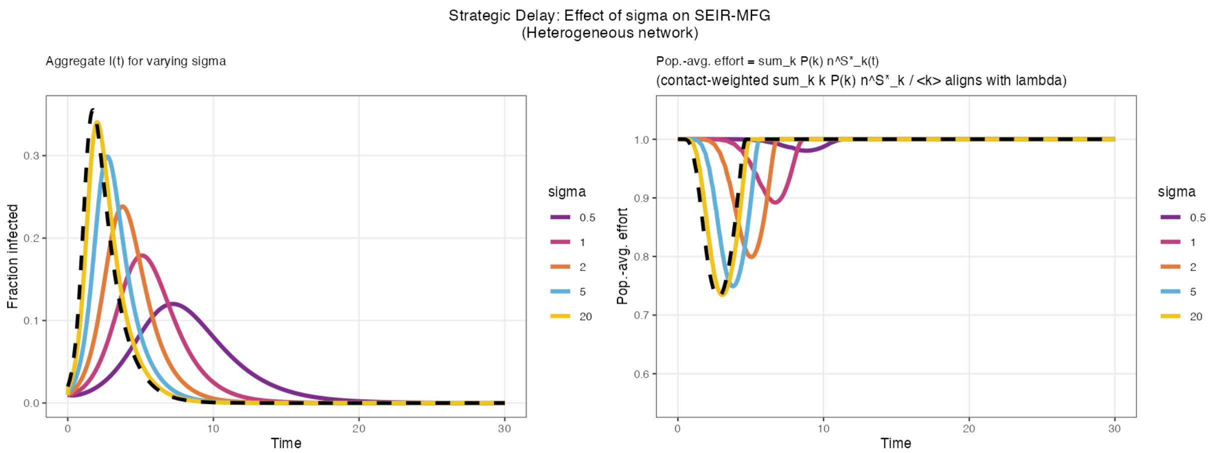

Figure 3. Effect of the incubation rate σ on the heterogeneous-network SEIR-MFG Nash equilibrium. **Left:** aggregate $I_{\mathrm{agg}}(t)$ for $\sigma \in \{0.5, 1, 2, 5, 20\}$ and the SIR limit (dashed black). In both panels the dashed black curve denotes the SIR limit ($\sigma \to \infty$). Decreasing σ delays and attenuates the epidemic peak. **Right:** population-average effort $\bar{n}^{S*}(t) = \sum_k P(k) n^{S*}_k(t)$. Longer incubation produces a shallower and later effort response, quantifying the strategic delay of Proposition 5.7. The non-monotone secondary adjustment visible for $\sigma = 0.5$ and $\sigma = 1$ arises from backward HJB propagation over a long epidemic horizon.

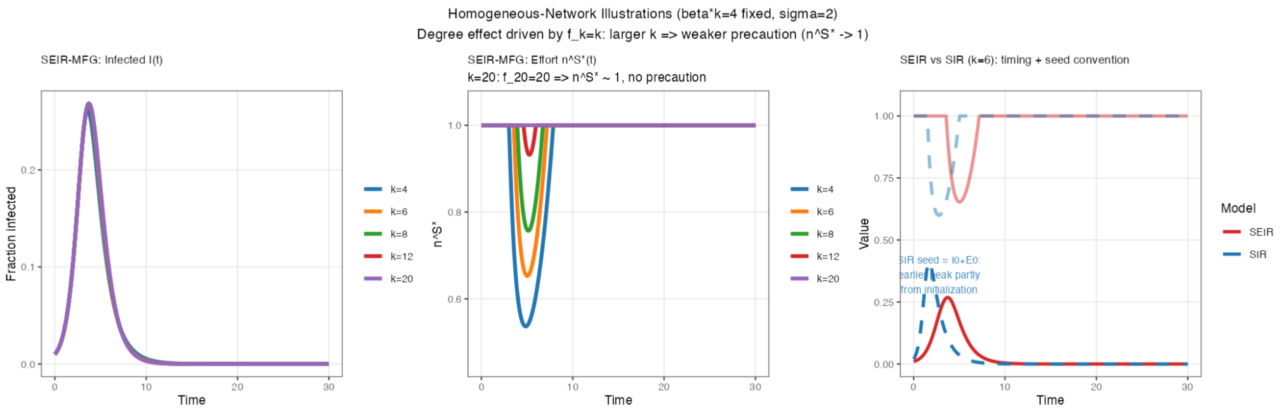

Figure 4. Homogeneous-network illustrations ($\beta k = 4$ fixed, $\sigma = 2$), presented as cost-normalization examples rather than validation of the full network model. **Left:** epidemic curves collapse across degree classes because βk is constant. **Center:** equilibrium effort profiles; larger k implies larger isolation cost $f_k = k$, and hence weaker precaution ($n_{20}^{S*} \equiv 1$, purple line at top). **Right:** SEIR vs. SIR comparison for $k = 6$; the earlier SIR peak is partly due to the seed convention $I_0^{\mathrm{SIR}} = I_0 + E_0$.

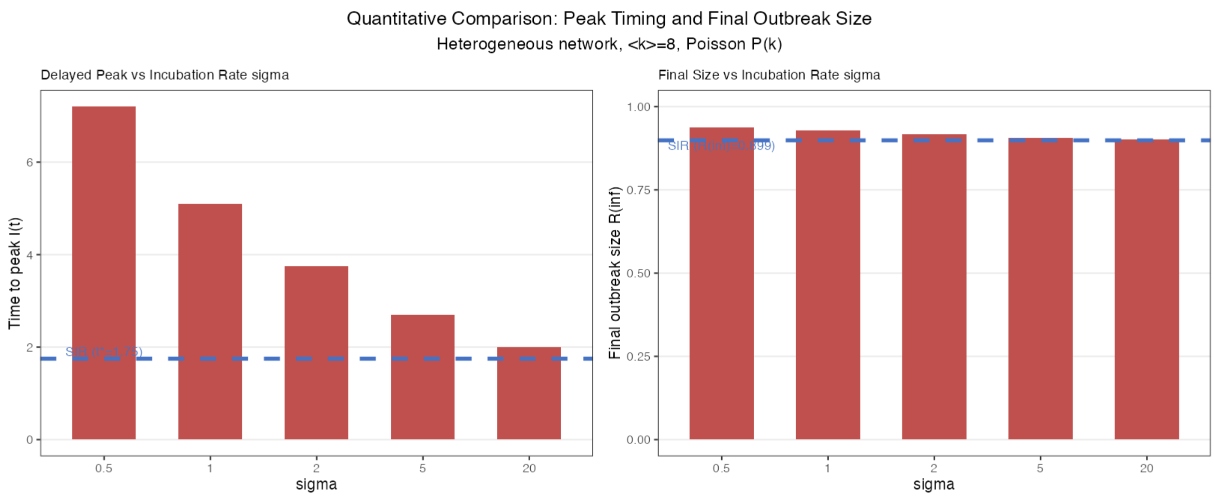

Figure 5. Quantitative summary for the heterogeneous-network SEIR-MFG across incubation rates σ (see Table 1). **Left:** time to aggregate peak t_{peak}; bars decrease monotonically from $\sigma = 0.5$ to the SIR reference (dashed blue), spanning a delay of more than a factor of four. **Right:** final outbreak size $R(\infty) = 1 - S_{\mathrm{agg}}(\infty)$; smaller σ produces a larger total outbreak despite a lower instantaneous peak, because weaker and later precaution allows more cumulative infections.

7. Conclusions and future directions

In this paper, we developed a mean-field game formulation for SEIR dynamics on heterogeneous contact networks with degree-dependent behavior. We derived the coupled forward–backward equilibrium system and obtained explicit best-response structure for susceptible contact effort under the convex isolation cost. A key qualitative consequence of the exposed compartment is that the incubation stage separates infection from infectiousness and shifts incentives over time; in the baseline formulation, exposed agents optimally maintain full contact, while susceptible agents reduce contact according to a value-gap criterion. We proved existence of equilibrium via a Schauder fixed-point argument and provided a uniqueness result under an appropriate monotonicity condition. Numerical experiments illustrate how degree heterogeneity, incubation, and the cost exponent influence equilibrium effort profiles and epidemic outcomes.

Several extensions are natural and would broaden the applicability of the framework. First, one can enrich the information structure: agents may observe only noisy aggregate signals, which leads to partially observed control and filtering-coupled HJB systems. Second, one can incorporate additional policy levers, including testing, isolation mandates, and contact tracing, which act directly on exposed individuals and create state-dependent constraints or penalties; this would clarify when and how nontrivial exposed effort can arise as an equilibrium outcome. Third, the network environment can be made time-dependent by allowing mobility-driven mixing or adaptive rewiring, so that contact opportunities evolve endogenously with perceived risk and public interventions. Fourth, heterogeneity beyond degree can be incorporated to study targeted incentives and distributional outcomes. Finally, empirical calibration and validation using behavioral and epidemic data would help identify which isolation-cost specifications reproduce observed contact reductions across connectivity classes.

Lastly, another future avenue will be incorporating more types of human behavior, such as compliance vs. noncompliance and age-structured population. The SIR-based models incorporating such behavior have been studied from various aspects including ODE, reaction-diffusion PDEs, optimal control, and stochastic differential equations [38–44].

Use of AI tools declaration

The authors declare they have not used Artificial Intelligence (AI) tools in the creation of this article.

Acknowledgments

This research was partially supported by the Simons Foundation Travel Support for Mathematicians (No. 0007730).

Conflict of Interest

The author declares that the research was conducted in the absence of any commercial or financial relationships that could be construed as a potential conflict of interest.

Data Availability Statement

This manuscript contains no experimental data. All numerical simulation results are reproducible from the model equations and parameter values reported in Section 6. The forward-backward sweep algorithm is described in full in Section 6 and can be implemented directly from the pseudocode provided therein. No external datasets were used. The simulation code that reproduces all figures and tables is publicly available at https://doi.org/10.5281/zenodo.19381052 and as an R package on CRAN (`install.packages("seirMFG")`).

References

1. W. O. Kermack, A. G. McKendrick, A contribution to the mathematical theory of epidemics, *Proc. R. Soc. Lond. A*, **115** (1927), 700–721. https://doi.org/10.1098/rspa.1927.0118
2. R. M. Anderson, R. M. May, *Infectious Diseases of Humans: Dynamics and Control*, Oxford University Press, Oxford, 1991.
3. S. Funk, M. Salathé, V. A. A. Jansen, Modelling the influence of human behaviour on the spread of infectious diseases: A review, *J. R. Soc. Interface*, **7** (2010), 1247–1256. https://doi.org/10.1098/rsif.2010.0142
4. F. Verelst, L. Willem, P. Beutels, Behavioural change models for infectious disease transmission: A systematic review (2010–2015), *J. R. Soc. Interface*, **13** (2016), 20160820. https://doi.org/10.1098/rsif.2016.0820
5. E. P. Fenichel, C. Castillo-Chavez, M. G. Ceddia, G. Chowell, P. A. G. Parra, G. J. Hickling, et al., Adaptive human behavior in epidemiological models, *Proc. Natl. Acad. Sci. USA*, **108** (2011), 6306–6311. https://doi.org/10.1073/pnas.1011250108
6. C. Eksin, J. S. Shamma, J. S. Weitz, Disease dynamics in a stochastic network game: A little empathy goes a long way in averting outbreaks, *Sci. Rep.*, **7** (2017), 44122. https://doi.org/10.1038/srep44122
7. T. C. Reluga, Game theory of social distancing in response to an epidemic, *PLoS Comput. Biol.*, **6** (2010), e1000793. https://doi.org/10.1371/journal.pcbi.1000793
8. C. T. Bauch, D. J. D. Earn, Vaccination and the theory of games, *Proc. Natl. Acad. Sci. USA*, **101** (2004), 13391–13394. https://doi.org/10.1073/pnas.0403823101
9. M. J. Keeling, K. T. D. Eames, Networks and epidemic models, *J. R. Soc. Interface*, **2** (2005), 295–307. https://doi.org/10.1098/rsif.2005.0051
10. M. E. J. Newman, Spread of epidemic disease on networks, *Phys. Rev. E*, **66** (2002), 016128. https://doi.org/10.1103/PhysRevE.66.016128
11. R. Pastor-Satorras, C. Castellano, P. Van Mieghem, A. Vespignani, Epidemic processes in complex networks, *Rev. Mod. Phys.*, **87** (2015), 925–979. https://doi.org/10.1103/RevModPhys.87.925
12. E. Volz, SIR dynamics in random networks with heterogeneous connectivity, *J. Math. Biol.*, **56** (2008), 293–310. https://doi.org/10.1007/s00285-007-0116-4
13. M. Boguñá, R. Pastor-Satorras, Epidemic spreading in correlated complex networks, *Phys. Rev. E*, **66** (2002), 047104. https://doi.org/10.1103/PhysRevE.66.047104

14. I. Z. Kiss, J. C. Miller, P. L. Simon, *Mathematics of Epidemics on Networks: From Exact to Approximate Models*, Springer, Cham, 2017. https://doi.org/10.1007/978-3-319-50806-1
15. J. M. Lasry, P. L. Lions, Mean field games, *Jpn. J. Math.*, **2** (2007), 229–260. https://doi.org/10.1007/s11537-007-0657-8
16. M. Huang, R. P. Malhamé, P. E. Caines, Large population stochastic dynamic games: Closed-loop McKean–Vlasov systems and the Nash certainty equivalence principle, *Commun. Inf. Syst.*, **6** (2006), 221–252.
17. R. Carmona, F. Delarue, *Probabilistic Theory of Mean Field Games with Applications II*, Springer Cham, 2018. https://doi.org/10.1007/978-3-319-56436-4
18. D. A. Gomes, J. Saúde, Mean field games models—a brief survey, *Dyn. Games Appl.*, **4** (2014), 110–154. https://doi.org/10.1007/s13235-013-0099-2
19. Y. Achdou, I. Capuzzo-Dolcetta, Mean field games: Numerical methods, *SIAM J. Numer. Anal.*, **48** (2010), 1136–1162. https://doi.org/10.1137/090758477
20. P. Cardaliaguet, S. Hadikhanloo, Learning in mean field games: The fictitious play, *ESAIM Control Optim. Calc. Var.*, **23** (2017), 569–591. https://doi.org/10.1051/cocv/2016004
21. R. Carmona, M. Laurière, Z. Tan, Model-free mean-field reinforcement learning: Mean-field MDP and mean-field Q-learning, preprint, arXiv:1910.12802.
22. R. Elie, E. Hubert, G. Turinici, Contact rate epidemic control of COVID-19: An equilibrium view, *Math. Model. Nat. Phenom.*, **15** (2020), 35. https://doi.org/10.1051/mmnp/2020022
23. S. Cho, Mean-field game analysis of SIR model with social distancing, preprint, arXiv:2005.06758.
24. L. Bremaud, D. Ullmo, Social structure description of epidemic propagation with a mean-field game paradigm, *Phys. Rev. E*, **106** (2022), L062301. https://doi.org/10.1103/PhysRevE.106.L062301
25. L. Bremaud, O. Giraud, D. Ullmo, Mean-field-game approach to nonpharmaceutical interventions in a social-structure model of epidemics, *Phys. Rev. E*, **110** (2024), 064301. https://doi.org/10.1103/PhysRevE.110.064301
26. L. Bremaud, O. Giraud, D. Ullmo, Mean-field game approach to epidemic propagation on networks, *Phys. Rev. E*, **112** (2025), L052301. https://doi.org/10.1103/mys6-fznc
27. C. Parkinson, S. Roy, A Fokker–Planck framework for control of epidemics, preprint, arXiv:2601.20181.
28. X. He, E. H. Y. Lau, P. Wu, X. Deng, J. Wang, X. Hao, et al., Temporal dynamics in viral shedding and transmissibility of COVID-19, *Nat. Med.*, **26** (2020), 672–675. https://doi.org/10.1038/s41591-020-0869-5
29. P. Brémaud, *Point Processes and Queues: Martingale Dynamics*, Springer, New York, 1981.
30. S. L. Chang, M. Piraveenan, P. Pattison, M. Prokopenko, Game theoretic modelling of infectious disease dynamics and intervention methods: A review, *J. Biol. Dyn.*, **14** (2020), 57–89. https://doi.org/10.1080/17513758.2020.1720322

31. H. Liu, X. Tian, Data-driven optimal control of a SEIR model for COVID-19, *Commun. Pure Appl. Anal.*, **22** (2023), 19–39. https://doi.org/10.3934/cpaa.2021093
32. J. Li, Z. Jin, M. Tang, Analysis of the SEIR mean-field model in dynamic networks under intervention, *Infect. Dis. Model.*, **10** (2025), 850–874. https://doi.org/10.1016/j.idm.2025.03.002
33. N. Sherborne, J. C. Miller, K. B. Blyuss, I. Z. Kiss, Mean-field models for non-Markovian epidemics on networks, *J. Math. Biol.*, **76** (2018), 755–778. https://doi.org/10.1007/s00285-017-1155-0
34. D. Xia, M. He, J. Mei, Q. Min, Physics-informed neural networks prediction approach for knowledge dissemination model considering knowledge media, *Knowl.-Based Syst.*, **324** (2025), 113514. https://doi.org/10.1016/j.knosys.2025.113514
35. J. Mei, R. Ye, Z. Xiang, J. Hu, W. Wang, A direct data-driven intermittent control and learning via Lyapunov-guided attraction region estimation with neural feedback loop design, *IEEE Trans. Autom. Sci. Eng.*, **23** (2026), 6504–6519. https://doi.org/10.1109/TASE.2026.3669581
36. E. Hubert, G. Turinici, Nash-MFG equilibrium in a SIR model with time dependent newborn vaccination, *Ricerche Mat.*, **67** (2018), 227–246. https://doi.org/10.1007/s11587-018-0365-0
37. A. Cecchin, M. Fischer, Probabilistic approach to finite state mean field games, *Appl. Math. Optim.*, **81** (2020), 253–300. https://doi.org/10.1007/s00245-018-9488-7
38. C. Parkinson, W. Wang, Analysis of a reaction-diffusion SIR epidemic model with noncompliant behavior, *SIAM J. Appl. Math.*, **83** (2023), 1969–2002. https://doi.org/10.1137/23M1556691
39. M. Bongarti, C. Parkinson, W. Wang, Optimal control of a reaction-diffusion epidemic model with non-compliance, *Eur. J. Appl. Math.*, **37** (2026), 313–338. https://doi.org/10.1017/S0956792525000130
40. C. Parkinson, W. Wang, A compartmental model for epidemiology with human behavior and stochastic effects, *Math. Biosci.*, **392** (2026), 109588. https://doi.org/10.1016/j.mbs.2025.109588
41. C. Ngo, C. Parkinson, W. Wang, Optimal control of an SIR model with noncompliance as a social contagion, preprint, arXiv:2509.09075.
42. G. Pang, É. Pardoux, PDE model for multi-patch epidemic models with migration and infection-age dependent infectivity, *Pure Appl. Funct. Anal.*, **9** (2024), 863–897.
43. G. Pang, É. Pardoux, SPDE for stochastic SIR epidemic models with infection-age dependent infectivity, *Stoch. Partial Differ. Equ. Anal. Comput.*, **14** (2026), 776–829. https://doi.org/10.1007/s40072-025-00403-x
44. G. Pang, É. Pardoux, A. Velleret, Stochastic SIR model with individual heterogeneity and infection-age dependent infectivity on large non-homogeneous random graphs, preprint, arXiv:2502.04225.